The Solidification and Aging Behavior of Types 308 and 308CRE Stainless Steel Welds

CRE additions to Type 308 stainless steel weld metal drastically alter precipitation reactions, resulting in an enhancement of elevated temperature properties

BY J. M. VITEK AND S. A. DAVID

ABSTRACT. Controlled residual element (CRE) additions of Ti, P, and B to Type 308 stainless steel filler metal have been previously shown to improve the elevated-temperature creep-rupture properties of welds. The solidification and aging behavior of Types 308 and 308CRE stainless steel welds were examined in an effort to identify the mechanism responsible for the improved mechanical properties.

Analysis of the as-welded microstructure and thermal analysis of the solidification behavior did not reveal any major differences that could be responsible for the creep-rupture improvement. However, extensive aging studies at 550 → 850°C (1022 → 1562°F) for times up to 10,000 hours revealed significant differences. The transformation of ferrite in the as-welded duplex structure to sigma phase was not retarded by CRE additions. However, the extensive precipitation of $M_{23}C_6$ at the austenite-ferrite interfaces in the aged Type 308 stainless steel welds was replaced by more homogeneous precipitation of titanium-rich carbides, nitrides, and sulfides in aged Type 308CRE stainless steel.

The results are summarized in the form of TTT diagrams. It is proposed that the elimination of a continuous network of carbides is responsible for the improved elevated-temperature properties. The different type of precipitate formed may also play a role.

Paper presented at the 64th Annual AWS Convention held in Philadelphia, Pennsylvania, April 24-29, 1983.

J. M. VITEK is a Research Staff Member and S. A. DAVID is Group Leader of the Welding and Brazing Laboratory, Metals and Ceramics Division, Oak Ridge National Laboratory, Oak Ridge, Tennessee.

Introduction

An investigation by Binkley *et al.* (Ref. 1) revealed that welds made with Type 308 stainless steel SMA electrodes with titania and lime-titania coatings had higher creep strength and ductility than welds made with lime-coated electrodes. Further work (Refs. 2,3) has shown that small additions of titanium, phosphorus, or boron to Type 308 stainless steel improve the elevated-temperature mechanical properties of this steel when in the welded condition. These additions have come to be known as controlled residual elements (CRE), and the modified steel is referred to in this paper as Type 308CRE stainless steel. The improved ductility was attributed to the absence of internal cracks in the Type 308CRE stainless steel welds (Ref. 3). These cracks were reported to be at austenite-sigma interfaces in Type 308 stainless steel welds after elevated temperature testing. However, the mechanism by which CRE additions improve the mechanical properties has, until now, not been understood. Although austenite-sigma phase interfaces exist in both alloys, the reason for the absence of cracks in Type 308CRE stainless steel weld metal is not known.

The investigation described here was undertaken to try to unravel the mystery of CRE additions and their effect on elevated temperature properties of austenitic stainless steel welds. The study examined two areas in which CRE additions may be influential. The solidification behavior of Types 308 and 308CRE stainless steels was followed, and the as-welded microstructures were compared.

The aging behavior of Types 308 and 308CRE stainless steel welds was also investigated. Since the CRE additions influence the mechanical properties after long-term exposure of the welds to elevated temperatures, it was felt that the effect of CRE additions may be greatest on the aging response of these alloys. In order to investigate the effect of CRE additions on the equilibrium structure of Type 308 stainless steel, a companion study was carried out on the aging behavior of homogenized Types 308 and 308CRE stainless steels. The results of this study are reported elsewhere (Ref. 4).

Experimental Procedure

The solidification behavior was investigated by carrying out differential thermal analysis (DTA) studies with a Mettler thermoanalyzer on samples of both Types 308 and 308CRE stainless steel filler metal. Chemical analyses of the stock used for DTA analysis (also used for making welds) are given in Table 1. Samples weighing 7 to 8 grams (g) were heated in an argon atmosphere to about 50°C (90°F) above the liquidus temperature and then cooled at a constant rate of 6°C/min (11°F/min). During cooling, a 12-channel compensated recorder traced the DTA curves.

The welds examined in this study were multipass welds deposited on a ½ in. (12.7 mm) thick Type 304L stainless steel plate (0.019 C, 1.75 Mn, 0.029 P, 0.006 S, 0.63 Si, 18.55 Cr, 10.0 Ni, bal Fe (in wt-%) containing a single V-groove butt joint. Welds were made using gas tungsten arc

Table 1—Compositions of Alloys Used in This Investigation

Material	Alloy	Welding process	Composition, wt-% C	Mn	Si	P	S	Cr	Ni	Ti	B	N_2
Filler	308	GTA/SA	0.065	1.52	0.44	0.022	0.008	20.51	10.53	-	-	-
Metal	308	SMA	0.047	1.77	0.34	0.023	0.013	20.75	9.74	-	-	-
	308CRE	GTA/SA	0.042	2.28	0.6	0.034	0.009	20.3	10.1	0.83	0.0033	-
	308CRE	SMA	0.055	1.78	0.5	0.04	0.006	19.4	9.25	0.06	0.008	-
Weld[a]	308	GTA	0.053[b]	1.75	0.46	0.018	0.008	20.21	9.36	<0.01	0.002	0.058
	308CRE	GTA	0.036	1.95	0.61	0.012	0.014	19.79	9.90	0.50	0.003	0.022

[a]As-welded (average of two welds analysis)
[b]This was the only case in which the two welds analyzed differed significantly. The two carbon levels were 0.037 and 0.068.

(GTA), submerged arc (SA), and shielded metal arc (SMA) processes. Compositions of the filler metals used as well as of the final welds are given in Table 1.

The aging studies were performed on the GTA welds only. The welds were cut from the welded plate and encapsulated in quartz tubes that were evacuated and refilled with a partial pressure of argon. Aging was at 550, 650, 750, and 850°C (1022, 1202, 1382, and 1562°F) for times of 0.3 to 10,000 hours (h). After aging, specimens were cut for extraction analyses, optical microscopy, and electron microscopy. Only the upper portion of the welds was used, avoiding possible dilution effects near the root of the welded multipass V-groove butt joints.

The transformation kinetics of ferrite within the aged welds was followed by measuring the magnetic permeability with a Magne-gage instrument. In order to minimize the effect of small variations in ferrite number from sample to sample, ferrite numbers were measured on each sample both before and after aging. The amount of ferrite remaining was always normalized to the value determined on the same sample before aging. The ferrite numbers were measured in accordance with AWS A4.2-74, *Standard Procedures for Calibrating Magnetic Instruments to Measure the Delta Ferrite Content of Austenitic Stainless Steel Weld Metal.*

The degree of precipitation as a function of aging was determined by extraction methods. Electrolytic extractions were made on samples with an approximate mass of 0.3 g. The extractions were performed at 1.5 volts (V) for 5 h in a 10% HCl-90% methanol solution using a platinum cathode. These conditions ensured selective removal of the matrix without any dissolution of carbides. The ferrite and sigma phases were also dissolved in the process. After rinsing and centrifuging the precipitates from the supernate, the precipitates were weighed in air and the weights were converted to weight-in-vacuum in order to correct for atmospheric variations. The reproducibility of the extraction results was determined previously (Ref. 5). A value of $\sigma = \pm 0.1$ wt-% was found for the range of 0–4 wt-% precipitate.

Microstructural analysis was done using a combination of optical microscopy and electron microscopy. Thin foil specimens were made from wafers sliced from the welds and subsequently electrodischarge machined into 3 mm (0.12 in.) diameter discs. The discs were then ground to a thickness of approximately 0.010 in. (0.25 mm) before being electrochemically polished. A JEOL 100CX transmission electron microscope equipped with an x-ray energy dispersive spectrometer (EDS) was used. The EDS data were used to assist in precipitate identification.

Results

Solidification Behavior

The DTA traces showing the heat release as a function of cooling time are shown in Fig. 1. The cooling time is proportional to the temperature since a constant cooling rate of 6°C/min (11°F/min) was used. For Type 308 stainless steel shown in Fig. 1A, the DTA thermogram for cooling of the specimen from the liquid state consists of two exothermic reactions that have been identified previously (Ref. 6). The first peak corresponds to primary ferrite (δ) solidification, beginning at 1435°C (2615°F). The second peak has been associated with the peritectic reaction liquid + ferrite → austenite (γ). This begins at 1387°C (2529°F), and solidification is complete at 1355°C (2471°F).

Table 2—Ferrite Numbers in As-Welded Microstructures

Welding process	Weld metal 308	308CRE
GTA	8.5	13.0
SA	8.0	7.5
SMA	7.0	3.5

The DTA curve for solidification of Type 308CRE stainless steel, shown in Fig. 1B, is similar to that for Type 308 stainless steel, with only a shift in the reaction temperatures. The liquidus, corresponding to primary ferrite solidification, occurs at 1440°C (2624°F). The peritectic reaction forming austenite occurs at 1355°C (2471°F), and the solidus is located at 1340°C (2444°F).

As-Welded Microstructures

The as-welded microstructures were examined optically, and the ferrite contents were measured. Ferrite numbers are given in Table 2. In general, the ferrite morphologies for the two alloys were similar. For SA and SMA welds, the ferrite morphology was vermicular for both

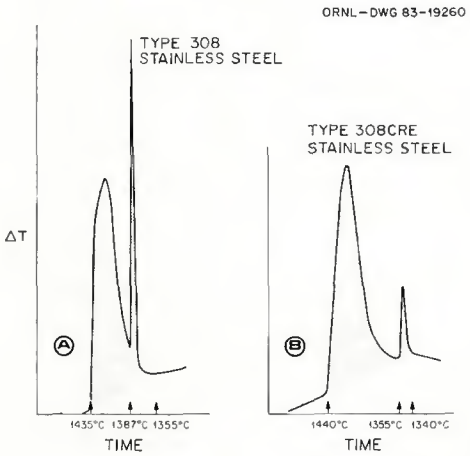

Fig. 1—Differential thermal analysis curves for cooling: A—Type 308 stainless steel; B—Type 308CRE stainless steel

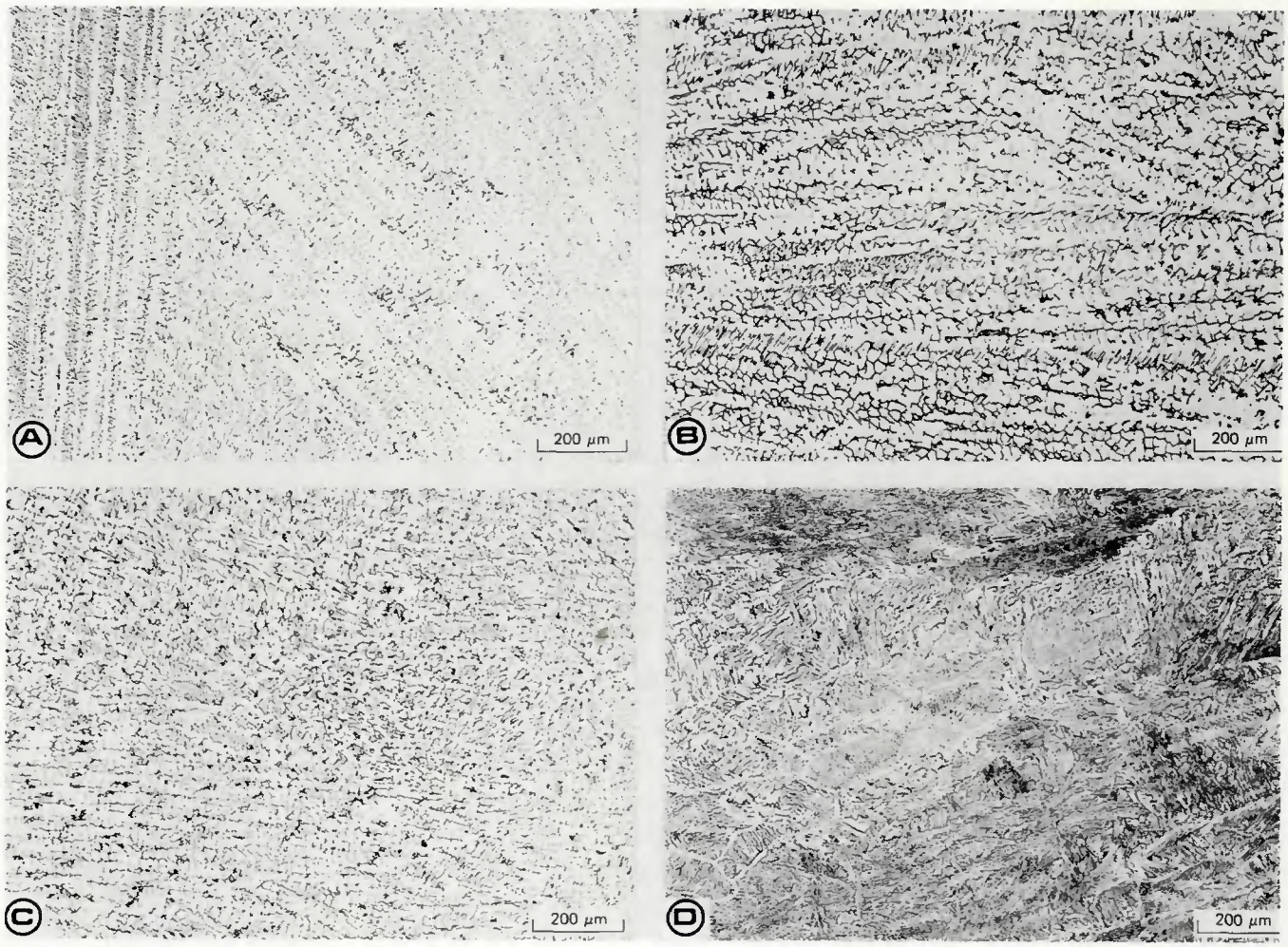

Fig. 2 — As-welded microstructures: A — Type 308 stainless steel submerged arc weld; B — Type 308CRE stainless steel submerged arc weld; C — Type 308 stainless steel gas tungsten arc weld; D — Type 308CRE stainless steel gas tungsten arc weld

Types 308 and 308CRE stainless steels. An example of the morphologies is given in Figs. 2A and 2B. In the case of the GTA welds, the Type 308CRE stainless steel welds had an acicular ferrite morphology, compared to the vermicular Type 308 stainless steel ferrite as shown in Figs. 2C and 2D.

Aging Studies

The transformation of ferrite was followed by monitoring the percent ferrite remaining after aging. The results for Types 308 and 308CRE stainless steels are presented in Figs. 3 and 4. Upon aging at 550°C (1022°F), the ferrite transformation in both steels is very slow. Approximately 80% of the ferrite remains after aging 1000 h at 550°C (1022°F). In contrast, the ferrite transformation is substantially faster after aging at 650, 750, or 850°C (1202, 1382, or 1562°F).

In the case of Type 308 stainless steel, the rate of the ferrite reaction is nearly the same at all three temperatures. Interestingly, the ferrite level decreases to approximately 60 to 70% within 1 h, while over 1000 h is required to reduce the residual ferrite to less than 10%.

The transformation kinetics of ferrite in the Type 308CRE stainless steel are more temperature sensitive, with the fastest rate of ferrite depletion at 750°C

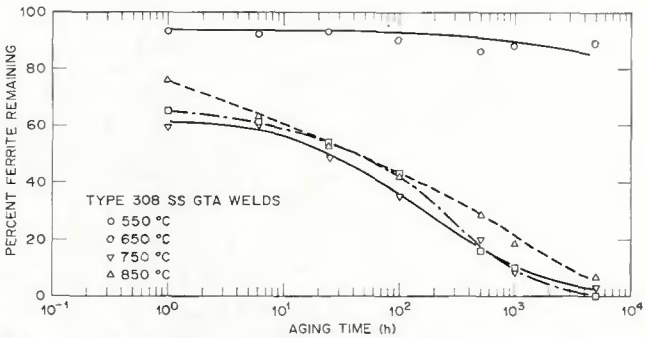

Fig. 3 — Plots of percent ferrite vs. aging time for aged Type 308 stainless steel welds

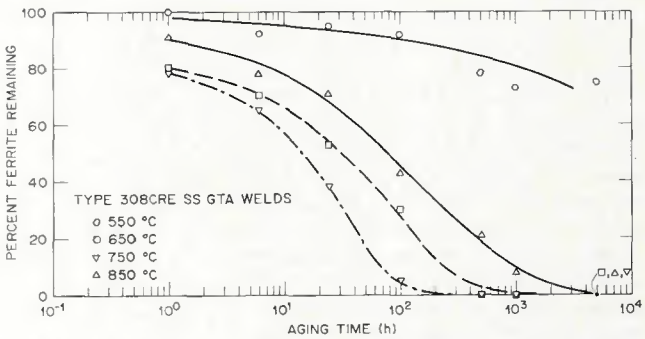

Fig. 4 — Plots of percent ferrite vs. aging time for aged Type 308CRE stainless steel welds

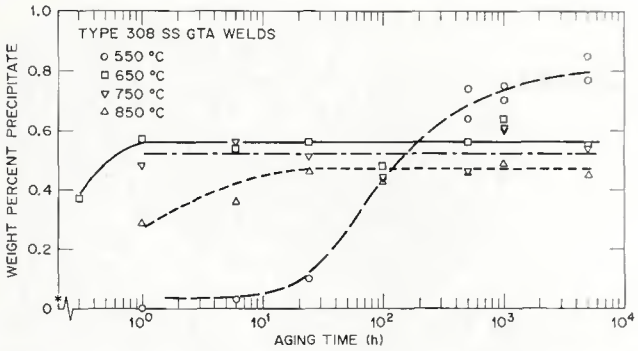

Fig. 5 — Weight-percent (wt-%) precipitate vs. aging time for aged Type 308 stainless steel welds

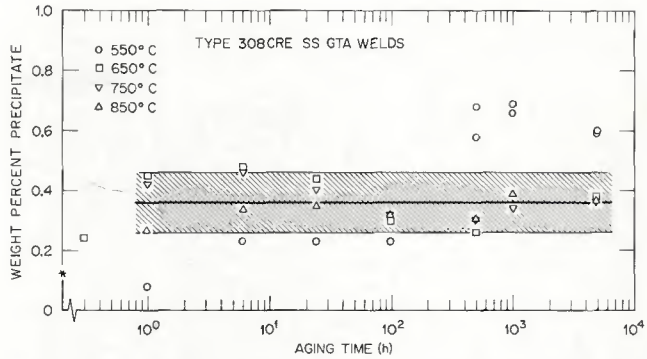

Fig. 6 — Weight percent (wt-%) precipitate vs. aging time for aged Type 308CRE stainless steel

(1382°F). The kinetics of ferrite depletion for Type 308CRE stainless steel are also faster than for Type 308 stainless steel, with 0% ferrite remaining after only 500 h at 650 or 750°C (1202 or 1382°F).

In addition to the depletion of ferrite upon aging, abundant precipitation occurs. The amount of precipitate was determined by electrolytic extractions and the results are given in Figs. 5 and 6 in the form of weight-percent (wt-%) precipitate vs. aging time curves. For Type 308 stainless steel welds, the amount of precipitate increased from an as-welded value of 0.04% to a value of ~0.50% after 1000 h. The precipitation reaction was quite fast at all aging temperatures except 550°C (1022°F). After only 1 h at 650 or 750°C (1202 or 1382°F), nearly all of the precipitate formed. X-ray diffraction and electron microscopy was used to identify the precipitate as chromium-rich $M_{23}C_6$.

Precipitation in Type 308CRE stainless steel welds was also found upon aging. From an as-welded value of 0.13 wt-% precipitate, an asymptotic value of approximately 0.4% was obtained within a few hours of aging at 650, 750, or 850°C (1202, 1382 or 1582°F). The precipitation reaction at 550°C (1022°F) was somewhat slower, requiring several hundred hours to reach completion. The precipitates were identified by x-ray diffraction and electron microscopy as primarily titanium carbides, nitrides, and sulfides. A small amount of $M_{23}C_6$ carbide was also detected.

The structural changes that occur upon aging may be followed by optical microscopy. Although the fine precipitates cannot be seen, the ferrite transformations can be followed. A typical series of micrographs showing the structural development after aging at 650°C (1202°F) is shown in Fig. 7 for Type 308 stainless steel and in Fig. 8 for Type 308CRE stainless steel.

The large-scale overviews shown in the optical micrographs of Figs. 7 and 8 reveal there are areas of ferrite that resist the transformation to sigma whereas other areas are completely transformed to sigma. This observation is particularly true for the Type 308 stainless steel even after aging times of 1000 h or more. Upon transforming to sigma, the ferrite morphology is maintained initially, but with further aging the sigma phase becomes consolidated into more spherically shaped grains.

Transmission electron microscopy (TEM) was also used to follow the structure of the welds as a function of aging. In the very early stages of aging of Type 308 stainless steel, two changes are readily apparent. At the original ferrite/austenite interface, the $M_{23}C_6$ precipitate forms, with a cube-on-cube orientation relationship with the austenite matrix. Simultaneously, the ferrite dissolves to a limited extent, leaving the residual ferrite enriched in chromium and depleted in nickel.

Figure 9 reveals the structure after short aging times; the original ferrite/austenite interface is clearly marked by the $M_{23}C_6$ precipitate. In some areas, where the ferrite is in the form of long thin fingers, the ferrite is completely dissolved and only the $M_{23}C_6$ carbide remains. The $M_{23}C_6$ identification was confirmed by electron diffraction analysis. EDS indicated the precipitate is substantially enriched in chromium. Upon further aging, the ferrite transforms to sigma phase, shown in Fig. 10. The nearly continuous network of carbides at the original austenite/ferrite interface is readily seen, as well as the receded ferrite boundary. Among the specimens aged for 500 h or more, the ferrite-to-sigma-phase transformation was never observed in an intermediate stage. Grains were found to be either all-ferrite or all-sigma with no partially transformed grains. In agreement with the optical microscopy results, some ferrite grains were found to remain untransformed even after aging for 1000 h. The residual ferrite grains were often heavily surrounded by $M_{23}C_6$, but this was not always the case.

The TEM examination of aged type 308CRE welds revealed quite a different sequence of reactions. Titanium-rich pre-

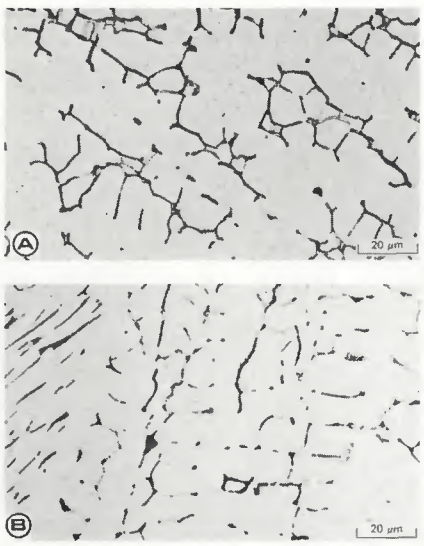

Fig. 7 — Optical micrograph of Type 308 stainless steel GTA welds aged at 650°C (1202°F): A — 1 h; B — 500 h

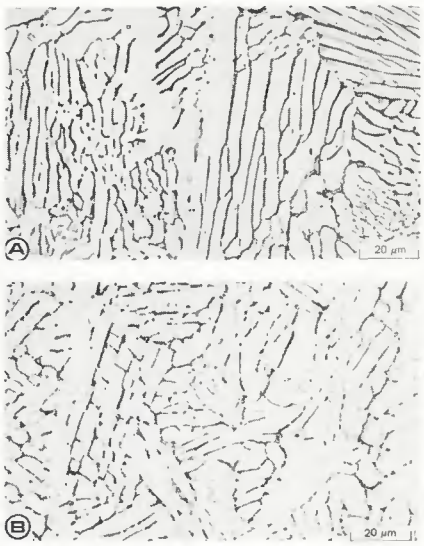

Fig. 8 — Optical micrograph of Type 308CRE stainless steel GTA welds aged at 650°C (1202°F): A — 1 h; B — 500 h

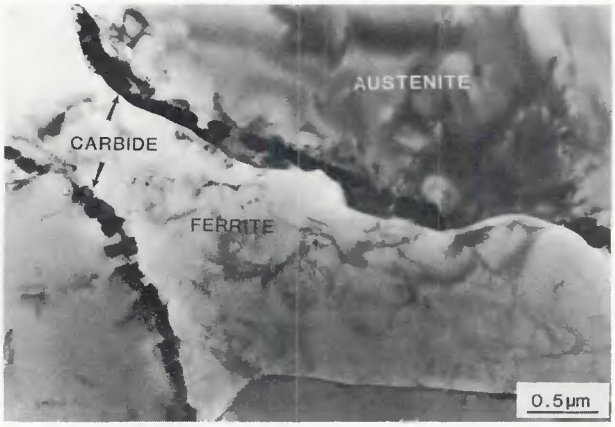

Fig. 9 — Electron micrograph of Type 308 stainless steel weld aged at 650°C (1202°F) for 18 min

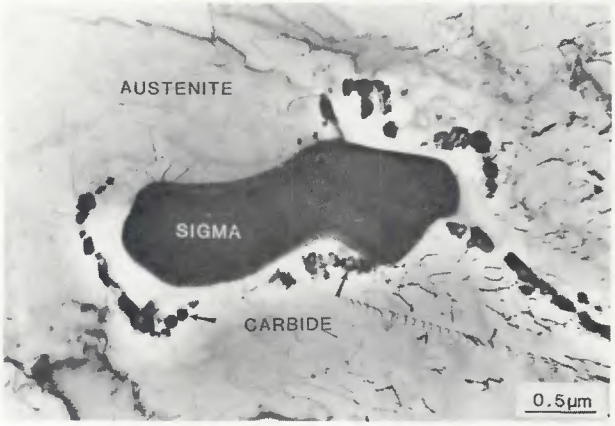

Fig. 10 — Electron micrograph of Type 308 stainless steel weld aged at 750°C (1382°F) for 100 h

cipitates formed during aging were observed to be distributed throughout the material: in the austenite matrix, at the austenite/ferrite interface, and sometimes even within the ferrite. Any precipitation at the austenite/ferrite interface is much finer and much less extensive than that found in aged Type 308 stainless steel weld metal. Furthermore, the formation of $M_{23}C_6$ carbide is significantly reduced. Only occasional $M_{23}C_6$ precipitates were observed.

In the early stages of aging, ferrite dissolution also occurred. Figure 11 shows the typical short-term aging microstructure. With further aging, the ferrite transforms to sigma phase — Fig. 12. The ferrite-to-sigma transformation is completed earlier in the aged Type 308CRE stainless steel welds than in the aged Type 308 stainless steel welds. No evidence of residual ferrite was found after aging the Type 308CRE stainless steel weld metal for 500 h at either 650 or 750°C (1202 or 1382°F).

The results of the aging studies have been summarized in the form of time-, temperature-, transformation (TTT) diagrams. These diagrams incorporate the results of optical and electron microscopy, measurements of residual ferrite levels, and electrolytic extraction data.

Figure 13 is the TTT diagram for Type 308 stainless steel, and Figure 14 is the TTT diagram for Type 308CRE stainless steel. Both diagrams are for material starting in the as-welded condition. The diagrams show the onset of precipitation, the beginning of the ferrite-to-sigma transformation, and the depletion of all the residual ferrite. It is clear from a comparison of Figs. 13 and 14 that the ferrite-to-sigma transformation is faster for the Type 308CRE stainless steel weld metal.

Discussion

CRE additions to Type 308 stainless steel filler metal affect the equilibrium phase stability relationships between ferrite and austenite. As shown in another study (Ref. 4), the titanium addition in particular stabilizes the ferrite phase at elevated temperatures so that, following a homogenizing treatment, a duplex ferrite plus austenite structure is found in Type 308CRE stainless steel compared to a single-phase austenite structure observed in homogenized Type 308 stainless steel. The titanium brings about this change because it is an intrinsic ferrite stabilizer. The ferrite-stabilizing tendency of titanium can help explain why the relative size of the first solidification peak in the DTA traces (Fig. 1), due to primary ferrite formation, is larger for Type 308CRE stainless steel.

Nevertheless, a comparison of types 308 and 308CRE welds shows no major differences. The DTA analysis indicates the solidification mode, primary ferrite formation, is similar and in most cases the weld morphologies are identical. Therefore, in agreement with Klueh and Edmonds (Ref. 7), it is concluded that CRE additions have only a minor influence on the as-welded structure of Type 308 stainless steel filler metal. In the case of SA and SMA welds, where the Types 308 and 308CRE stainless steel weld microstructures are similar, as well as for GTA welds in which the duplex structure morphologies differ slightly, improved elevated temperature creep properties are noted for Type 308CRE stainless steel welds.

It may be concluded that any minor alterations in the weld microstructure of Type 308CRE stainless steel, if they exist

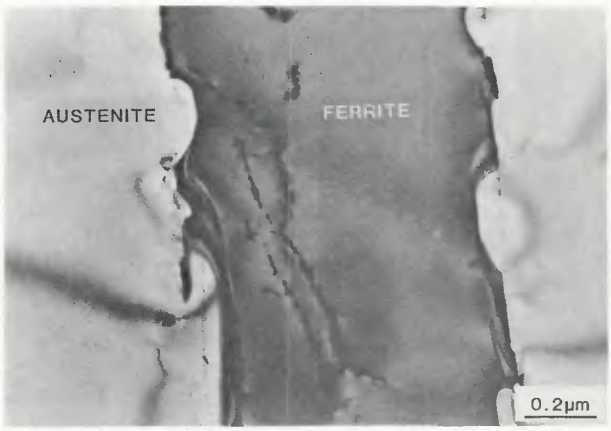

Fig. 11 — Electron micrograph of Type 308CRE stainless steel weld aged at 650°C (1202°F) for 1 h

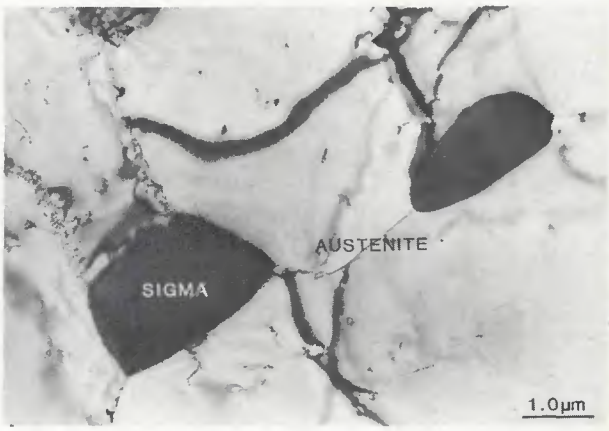

Fig. 12 — Electron micrograph of Type 308CRE stainless steel weld aged at 750°C (1382°F) for 1000 h

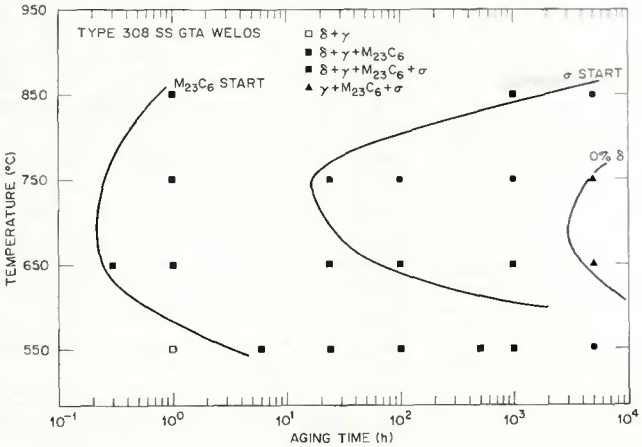

Fig. 13 — Time-temperature transformation curve for welded and aged Type 308 stainless steel

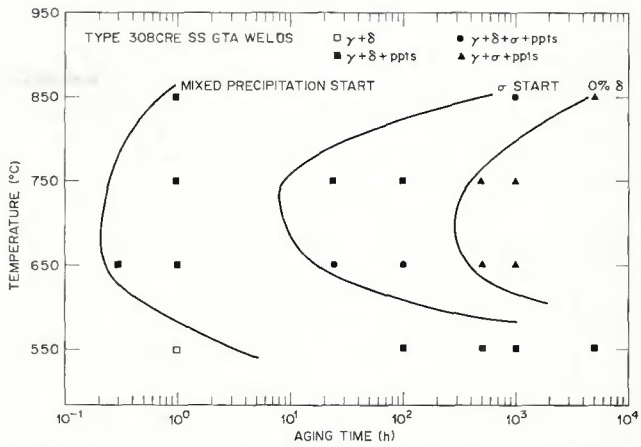

Fig. 14 — Time-temperature transformation curve for welded and aged Type 308CRE stainless steel

at all, cannot account for the improvement in mechanical properties. Rather, the beneficial effects of CRE additions must be due to the influence of these modifications on the long-term elevated temperature phase stability of Type 308 stainless steel welds. Consequently, the remainder of this discussion concentrates on the aging behavior of these two alloys, with the goal of trying to explain how CRE additions may improve the elevated temperature mechanical properties.

Upon elevated temperature exposure, two structural changes occur in the Types 308 and 308CRE stainless steel welds. First, significant precipitation occurs; this is discussed later. The second reaction is the elimination of the ferrite in the duplex weld microstructure. The ferrite phase found in the as-welded structures is metastable. Upon elevated temperature aging, the ferrite level decreases by two mechanisms:

1. The partial dissolution of ferrite.
2. Transformation of ferrite to sigma phase.

The former process occurs relatively quickly. Evidence of this dissolution process is shown by the rapid decrease in percent ferrite remaining as a function of aging (Figs. 3 and 4) and by the microstructure in Fig. 9. At 650 to 850°C (1202 to 1582°F), the ferrite level decreases by nearly 40% within the first hour of aging; this is associated with the ferrite dissolution reaction.

It was shown previously (Ref. 8) that the ferrite dissolution may lead to chromium enrichment and nickel depletion of the residual ferrite. Thermodynamic considerations limit the degree of chromium enrichment (or nickel depletion) possible, and it is suggested that due to this constraint the ferrite dissolution reaction reaches completion after relatively short aging times. With additional aging, any further depletion of ferrite occurs by the transformation of ferrite to sigma. Presumably, this reaction is enhanced kinetically by the chromium enrichment that occurs earlier. Thus, a two-step reduction in ferrite level vs. aging time is expected; this is observed in Figs. 3 and 4.

In the aging of Type 308 stainless steel welds, extensive carbide formation occurs at the ferrite/austenite interface. Since the $M_{23}C_6$ carbide formed is enriched in chromium, this precipitation process acts as another means by which the excess chromium is removed during the initial ferrite dissolution reaction. Evidence in support of this conclusion can be found by comparing the aging curves for Types 308 and 308CRE stainless steel welds in Figs. 3 and 4, respectively. The early ferrite depletion is much more extensive for Type 308 stainless steel, reducing the ferrite level by ~40% vs. only ~20% in type 308CRE stainless steel.

It was noted that some ferrite grains remained untransformed even after 1000 h of aging, whereas other ferrite grains transformed to sigma phase within less than 100 h. This large range of aging times applies to the aged Type 308 stainless steel; the range is considerably reduced for Type 308CRE stainless steel welds. At present it is not known why some ferrite grains resist transforming to sigma for extended periods. It is apparently not related to the extensive interface carbide formation in aged Type 308 stainless steel, since residual ferrite grains may or may not be surrounded by this carbide. The observations suggest the ferrite-to-sigma transformation is dictated by very slow nucleation, with subsequent growth of sigma in ferrite being rapid. This conclusion agrees with the well-known observation that the ferrite-to-sigma transformation is a very sluggish reaction.

Previous studies on the effects of CRE additions on Type 308 stainless steel filler metal have concentrated on mechanical properties (Refs. 1-3, 7). Improvements in elevated temperature creep ductility are the most noteworthy. However, very little work has been done to understand how CRE additions lead to such improvements in mechanical properties. Stiegler *et al.* (Ref. 3) noted that aged Type 308 stainless steel welds exhibited internal cracks at the sigma-austenite interfaces but such cracks were absent in aged Type 308CRE stainless steel welds. However, no detailed explanation was given as to why cracks formed in one alloy and not in the other.

The present results help to understand the role of CRE additions, and specifically titanium additions, in improving properties. Based on the present results, it is apparent that the titanium does not retard the ferrite-to-sigma transformation. Stiegler *et al.* (Ref. 3) suggested CRE additions slowed the sigma formation. However, our results show that, in the aged Type 308CRE stainless steel weld, the transformation of ferrite is in fact faster. At 750°C (1382°F), some ferrite remains in the Type 308 steel after 1000 h but all the residual ferrite has transformed in Type 308CRE stainless steel after only 500 h. The faster transformation rate of ferrite to sigma may be due, in part, to the absence of $M_{23}C_6$ carbide in aged Type 308CRE stainless steel welds. The $M_{23}C_6$ carbides are chromium-rich and undoubtedly compete with the sigma phase for the chromium available in the ferrite.

The present study shows a major influence of titanium on the precipitation reactions that occur. A similar effect of titanium on precipitation process was also found on aged but initially homogenized material (Ref. 4). The morphology, character, and distribution of the precipitates are quite different in the two alloys. In Type 308CRE stainless steel welds, the precipitates are distributed in a random fashion, whereas in Type 308 stainless steel welds, carbides form a network throughout the austenite matrix.

The network formed as described above is extensive and interconnected, following the outline of the ferrite/austenite interfaces in the as-welded state. The $M_{23}C_6$ carbides are quite stable, with no evidence of carbide dissolution as noted by others (Ref. 2). It is quite conceivable that such a network of precipitates would be very susceptible to crack formation and propagation. The carbides cannot be observed by optical microscopy. Therefore, it is possible the internal cracking observed optically at the sigma/austenite interfaces (Ref. 3) may have been displaced slightly from the actual interface and instead may have followed the carbide network path. A program is currently under way using interrupted creep specimens to evaluate this hypothesis. The role of titanium in improving creep ductility may also derive from the type of precipitation that occurs. Titanium nitrides and sulphides form, in addition to titanium carbides. It is possible the titanium scavenges undesirable elements, sulphur in particular, which otherwise may accumulate at the sigma/austenite interface.

There are experimental observations that support each of these proposed mechanisms by which titanium improves the elevated temperature creep properties. Stiegler *et al.* (Ref. 3) noted that internal cracks formed only in areas where the ferrite had transformed to sigma. This observation is compatible with the latter mechanism and indicates undesirable constituents such as sulphur might be rejected at the sigma/austenite interface during the ferrite-to-sigma transformation. Such a mechanism is also consistent with hypotheses relating to hot-cracking phenomena.

It is often proposed that primary ferrite formation reduces hot-cracking tendencies by limiting the segregation of undesirable constituents such as sulphur during solidification. Thus, the ferrite would be enriched in such elements, and these may be rejected during subsequent transformations. However, microscopy results do not completely agree with such a mechanism for two reasons:

1. The titanium precipitates are found throughout the structure and are not heavily concentrated near the ferrite areas.

2. The precipitation reactions occur early during aging; no substantial precipitation takes place when the ferrite transforms to sigma, at which time tramp constituents are presumably rejected.

Of course, it is possible that both mechanisms play a role. Internal cracking may initiate at the sigma interfaces where tramp elements might tend to segregate, and the $M_{23}C_6$ carbide network may provide a vulnerable path for crack propagation. These remaining questions will hopefully be resolved by the interrupted creep tests currently under way. In addition, further work on the distribution of each of the various titanium precipitates may be warranted. Nevertheless, it is clear that titanium's role in improving the creep properties is in the precipitation process; it has no beneficial effect on the formation or the kinetics of formation of sigma phase.

Based on the extraction results, some insight into the amount of titanium needed as CRE additions may be gained. Other work (Ref. 9) indicates the titanium carbides, nitrides and sulphides are most likely TiC, TiN, and $Ti_4C_2S_2$, respectively. From the chemical analyses of the GTA welds (Table 1), the Type 308CRE stainless steel welds contained on average 0.036% C, 0.014% S, and 0.022% N.

One can assume that all the sulphur and nitrogen are tied up as $Ti_4C_2S_2$ and TiN, respectively, and that the remaining carbon is tied up as TiC. Given this assumption, one can calculate the amount of precipitate expected as well as the amount of titanium needed. Such calculations predict that 0.31 wt-% precipitate should form, compared to the ~0.4 wt-% found.* Thus, agreement is relatively good and the assumptions seem valid.

The amount of titanium needed to produce 0.31 wt-% of precipitate is 0.24%, substantially below the 0.50% in the alloy. Only a limited amount of titanium is expected to be in solution, therefore, the Type 308CRE stainless steel welds may contain an excess of titanium. It is interesting to note that other work (Ref. 1) has shown the optimum titanium level for SA and SMA welds is 0.2%; this is very close to the value calculated that is needed to tie up all the carbon, nitrogen, and sulphur.

Similar calculations can be made to determine how much of the carbon is tied up as $M_{23}C_6$ in the aged Type 308 stainless steel welds. If all of the 0.5 wt-% precipitate found in these aged welds is assumed to be $M_{23}C_6$, then one would need 0.028% carbon in the alloy.† One weld analysis indicated 0.037% carbon was present, close to the calculated value and suggesting nearly all the carbon is tied up as carbide. However, the other weld analysis indicated 0.068% carbon was present. This higher carbon value is identical to the carbon content in the filler metal used for the welds and may indicate a large variation in carbon retention from weld to weld.

**If it is assumed some carbide was in the form of $M_{23}C_6$, the 0.31 wt-% value would increase somewhat.*

†This calculation is based on the assumption that the carbide stoichiometry is $(Cr_{16}Fe_7)\ C_6$.

Some of the features of the TTT diagrams presented in Figs. 13 and 14 may be compared to TTT diagrams developed by others (Refs. 10, 11) for Types 316 and 321 austenitic stainless steels. Very rapid precipitation of $M_{23}C_6$ was noted for Type 316 stainless steel (Ref. 11), in agreement with our results. Grot and Spruiell (Ref. 10) found that titanium additions delayed and retarded the nucleation and growth of $M_{23}C_6$. Our results indicate that a major portion of the $M_{23}C_6$ precipitate formation was replaced, rather than delayed, by titanium precipitate formation.

Grot and Spruiell also noted that titanium additions to Type 316 stainless steel enhanced the kinetics of intermetallic phase formation, including σ phase formation. Our results agree with this observation. The ferrite-to-sigma transformation is completed in considerably less time in the titanium-modified Type 308 stainless steel than in the unmodified alloy.

Conclusions

The solidification behavior of Types 308 and 308CRE stainless steels was examined. In addition, the weld microstructures and aging behavior of welds of these two steels were also studied. Based on these investigations, the following conclusions have been drawn:

1. CRE additions do not alter the solidification mode, although they do result in greater ferrite stability.

2. The weld microstructures in SA and SMA welds are unchanged by CRE addition. For GTA welds, the Type 308CRE stainless steel has an acicular ferrite morphology compared to the vermicular ferrite morphology in Type 308 stainless steel. It is concluded that the improved elevated-temperature mechanical properties of Type 308CRE stainless steel cannot be attributed to modifications in the weld microstructures.

3. Aging studies in the temperature range of 550-850°C (1022-1582°F) have shown that CRE additions do not retard the ferrite-to-sigma phase transformations; instead they enhance the kinetics of the transformations slightly.

4. CRE additions significantly reduce the amount of $M_{23}C_6$ carbide precipitation. These precipitates are replaced by titanium-rich carbides, nitrides, and sulfides.

5. The distribution of precipitates in aged weld metal is dramatically altered by CRE additions. Whereas $M_{23}C_6$ forms primarily at prior ferrite/austenite boundaries in Type 308 stainless steel, the precipitates formed in aged Type 308CRE weld metal are more uniformly distributed throughout the matrix.

6. The improved elevated-tempera-

ture creep-rupture properties of Type 308CRE stainless steel weld metal are attributed to the altered precipitate distribution and/or the types of precipitates formed.

Acknowledgments

The authors would like to acknowledge W. H. Smith, S. E. Hanzelka, and R. W. Reed for preparing specimens and for their general technical support. Their assistance was invaluable in carrying out this research. The authors also wish to acknowledge the help of J. F. Young and F. A. Scarboro for the preparation of the manuscript. This research was sponsored by the Division of Materials Sciences, United States Department of Energy under contract W-7405-eng-26 with the Union Carbide Corporation.

References

1. Binkley, N. C., Berggren, R. G., and Goodwin, G. M. 1974. Effects of slight compositional variation on type E308 electrode deposits. *Welding Journal* 53(2): 91-s to 95-s.

2. King, R. T., Stiegler, J. O., and Goodwin, G. M. 1974. Relation between mechanical properties and microstructure in CRE type 308 weldments. *Welding Journal* 53(7): 307-s to 313-s.

3. Stiegler, J. O., King, R. T., and Goodwin, G. M. 1975. Effect of residual elements on fracture characteristics and creep ductility of type 308 stainless steel weld metal. *J. Eng. Mater. Technol.* 97(3): 245-250.

4. Vitek, J. M., and David, S. A. 1982. The effect of controlled residual elements on type 308 stainless steel weld metal structures. Paper presented at the 63rd Annual AWS Convention held in Kansas City, Missouri, during April 25-30, 1982.

5. Vitek, J. M., and Klueh, R. L. 1983. Precipitation reactions during the heat treatment of ferritic steels. *Metall. Trans. A 14A:* 1047-1055.

6. David, S. A., Goodwin, G. M., and Braski, D. N. 1979. Solidification behavior of austenitic stainless steel filler metals. *Welding Journal* 58(11): 330-s to 336-s.

7. Klueh, R. L., and Edmonds, D. P. 1983 (May). *Chemical composition effects on the creep of austenitic stainless steel weld metals.* ORNL-5840, Oak Ridge, Tennessee: Oak Ridge National Laboratory.

8. Vitek, J. M., and David, S. A. 1982. Microstructural analysis of austenitic stainless steel laser welds, *Trends in welding research in the United States,* ed., S. A. David, pp. 243-258. Metals Park, Ohio: American Society for Metals.

9. Leitnaker, J. M., and Gehlbach, R. E. *Thermodynamics of precipitation reactions in titanium-modifed stainless steel.* ORNL-TM-4543. Oak Ridge, Tennessee: Oak Ridge National Laboratory.

10. Grot, A. S., and Spruiell, J. E. 1975. Microstructural stability of titanium-modified type 316 and type 321 stainless steel. *Metall. Trans. A. 6A:* 2023-2030.

11. Weiss, B., and Stickler, R. 1972. Phase instabilities during high temperature exposure of 316 austenitic stainless steel. *Metall. Trans. 3: 851-866.*

WRC Bulletin 292
February, 1984

PVRC Milestone Gasket Tests—First Results
by M. Bazergui and L. Marchand

The Milestone Gasket Test Program is part of the Long Range Flanged Joint Improvement Program of the Pressure Vessel Research Committee. This paper presents an overview of the test program, provides details on the test setup, test procedure and leak rate determination.

Publication of this report was sponsored by the Subcommittee on Bolted Flanged Connections of the Pressure Vessel Research Committee of the Welding Research Council.

The price of WRC Bulletin 292 is $13. 50 per copy, plus $5.00 for postage and handling. Orders should be sent with payment to the Welding Research Council, Room 1301, 345 E. 47th St., New York, N. Y. 10017.

WRC Bulletin 284
April, 1983

The External Pressure Collapse Tests of Tubes

by E. Tschoepe and J. R. Maison

An experimental program was performed to confirm or refute the applicability of Figure UG-31 in Section VIII, Division 1 of the ASME Boiler and Pressure Vessel Code to the design of tubes under external pressure. Commercially available tubes were subjected to external pressure until collapse occurred. The data generated indicates the current ASME design rules for tubes under external pressure are suitable for continued application.

Publication of this report was sponsored by the Subcommittee on Shells of the Pressure Vessel Research Committee of the Welding Research Council.

The price of WRC Bulletin 284 is $12.00 per copy, plus $5.00 for postage and handling. Orders should be sent with payment to the Welding Research Council, Room 1301, 345 East 47th St., New York, NY 10017.